Hindawi
Science and Technology of Nuclear Installations
Volume 2023, Article ID 6363270, 10 pages
https://doi.org/10.1155/2023/6363270

Research Article

Detecting Unauthorized Movement of Radioactive Material Packages in Transport with an Adam-Optimized BP Neural Network Model

Panpan Jiang,[1,2,3] **Xiaohua Yang**,[3,4] **Yaping Wan**,[3,4] **Tiejun Zeng**,[3] **Mingxing Nie**,[3,4] **Chaofeng Wang**,[3,4] **Yu Mao**,[3,4] **and Zhenghai Liu**[3,4]

[1]*School of Nuclear Science and Technology, University of South China, Hengyang 421001, China*
[2]*School of Civil Engineering, University of South China, Hengyang 421001, China*
[3]*Intelligent Nuclear Security Technology Laboratory, Hengyang 421001, China*
[4]*School of Computer, University of South China, Hengyang 421001, China*

Correspondence should be addressed to Xiaohua Yang; xiaohua1963@usc.edu.cn and Yaping Wan; wypusc2023@126.com

Received 2 October 2023; Revised 4 December 2023; Accepted 5 December 2023; Published 18 December 2023

Academic Editor: Mark Deinert

Copyright © 2023 Panpan Jiang et al. This is an open access article distributed under the Creative Commons Attribution License, which permits unrestricted use, distribution, and reproduction in any medium, provided the original work is properly cited.

The rapid expansion of nuclear technology across various sectors due to global economic growth has led to a substantial rise in the transportation of radioactive materials. The International Atomic Energy Agency (IAEA) estimates that approximately 20 million shipments of radioactive materials occur annually. In this context, ensuring the safety and security of radioactive material transportation is of significant importance. IAEA's "Security of Radioactive Materials in Transport" (Nuclear Security Series No. 9-G) mandates that an effective transport security system should provide immediate detection of any unauthorized removal of the packages. In the present study, an innovative Adam-optimized BP neural network model is developed for detecting unauthorized movements of radioactive material packages. To analyze the performance of the proposed algorithm, numerous experiments were conducted. The results demonstrate that the proposed method achieves a 99.17% accuracy rate in detecting unauthorized movements of radioactive materials, with a missed alarm rate of 0.72% and a false alarm rate of 0.1%. This method also enables real-time detection of unauthorized removal of radioactive materials and effectively enhances the security of radioactive materials during transport to reduce the risks of theft, loss, diversion, or sabotage.

1. Introduction

Transporting radioactive materials is a crucial and integral aspect of the nuclear energy industry. Based on estimations conducted by the International Atomic Energy Agency (IAEA), approximately 20 million packages of radioactive materials, including UF6, radioactive sources, fissionable ores, spent fuel, and nuclear waste, are transported globally each year [1]. Typically, these materials are transported long distances and across large geographic areas, often spanning provinces or borders. However, the transportation of radioactive materials confronts some limitations in security and response forces. Consequently, it is crucial not to rely solely on security personnel or local police to handle unexpected and malicious incidents during the transportation of these hazardous materials. According to the records of the IAEA Incident and Trafficking Database (ITDB), 52% of all thefts of radioactive materials between 1993 and 2022 occurred during authorized transport. This figure has increased to 62% in the last decade [2]. Moreover, the event report website of the United States Nuclear Regulatory Commission (U.S.NRC) contains a substantial number of reports on the radioactive material lost during transit. For instance, on February 7, 2020, an Ir-192 source with a dose of 9.987 Ci was lost during transportation to Golden, Colorado [3]. On July 2, 2019, a moisture/density gauge (CPN International MC Series) that contained a 50 mCi Am-Be source and a 10 mCi Cs-137 source was lost

on the highway between Aurora and Columbus, Nebraska [4]. If not detected and responded to effectively, the loss or theft of radioactive materials can cause severe environmental contamination and public panic. Criminals may even use stolen radioactive materials for malicious purposes such as creating improvised nuclear devices (IND), radiological exposure devices (RED), radiological dispersal devices (RDD), and dirty bombs [5]. On the other hand, a widespread nuclear material leakage could lead to severe social and economic consequences and could easily kick off global anxiety and concerns [6]. Thus, further surveillance measures of nuclear materials lead to less risk and enhance global transportation security measures for radioactive materials.

In July 2020, the IAEA issued the latest implementing guide under the heading "Security of Radioactive Materials in Transport" [7]. This comprehensive and authoritative document guides the safe and secure transport of radioactive materials and mandates states to establish effective national nuclear security regimes. Based on this guide, transport security objectives are classified into basic, enhanced, and additional transport security levels. The security objectives are clearly defined for each level. According to the guide, the basic level requires detecting any unauthorized access or movement of packages. In this regard, the present study aims to focus on detecting unauthorized movements, also called illegal movement, of packages during the transportation of radioactive materials to prevent loss, theft, diversion, or sabotages.

2. Related Work

Recently, numerous studies have been conducted on detecting and tracking nuclear materials within facilities or during transportation. For instance, Gilbert et al. [8] employed spectral X-ray radiography to examine radioactive materials in packages or composite objects, aiming to disrupt the illicit trafficking of nuclear materials. Argonne National Laboratory developed an ARG-US system [9–11], which uses a range of sensors and active RFID tags to monitor real-time radiation dose, container sealing, as well as ambient temperature and state parameters of containers carrying radioactive materials. The system utilizes GPS technology to track and monitor vehicles transporting the materials. Additionally, the ARG-US system could be implemented for tracking and monitoring nuclear materials within facilities [12]. Vander Wal et al. [13] developed the TRAVELER program based on the ARG-US system and established a virtual geographic boundary for radioactive material shipments. The software automatically triggers an alarm if the transport vehicle leaves the electronic fence. Deb [14] proposed a method called the interior point method (IPM) to estimate the location and trajectory of a moving radioactive source. Moreover, Bauk [15] employed RFID technology and established a tracking model for radioactive materials during sea transportation. The model transmits diverse data including the latitude, longitude, speed, heading of the ship, and the radiation dose of cargo packages to ground-based control centers every two hours.

Several investigations have focused on detecting radioactive sources diverted illicitly in urban environments, which is an important part of modern nuclear security. A prefilter framework was presented for mobile sensor networks to estimate urban sources' positions and intensity [16]. When detecting illicit radioactive sources in urban areas, the performance of mobile detector systems is constrained by environmental interference. Thus, to address this challenge, the RadMAP system systematically probes variations in natural radiological background and creates multisensor datasets for mobile radiation detection [17]. A network of mobile distributed sensors was deployed on a vehicle platform to detect mobile radioactive sources. It was found that the detection time of mobile radioactive sources was affected by the speed of the source and the number of mobile detectors [18]. Studies [19] demonstrated that the fusion of extensive data generated by radiation detectors employing Pearson's methodology significantly enhances the source detection effectiveness of mobile radioactive materials.

When transportation occurs, vehicles may pass through tunnels, bridges, or remote mountainous areas, where GPS may not provide real-time location data. Meanwhile, cameras may not be applicable on ships to monitor radioactive materials due to confidentiality and privacy requirements. To address these challenges, Zeng et al. [20, 21] developed a method to detect unauthorized movements by installing a wireless node on radioactive items within the cargo package. In this context, Zeng et al. [20] established a network comprising numerous wireless nodes on the packages. In this approach, any illegal movement of containers can be detected by monitoring the real-time connection status between the detecting node and its adjacent nodes. If a node fails to communicate with its neighboring nodes during transportation, the system automatically issues an alarm indicating that the package has been lost or stolen. However, this method required a stable and reliable network between the nodes. More specifically, the system will generate false alarms if the network fails and communication breaks down. To resolve this shortcoming, the authors in [21] developed an illegal movement detection model based on a space triangle. This approach involves three steps: 1. the received signal strength indicator (RSSI) values were calculated by measuring the signal strength between the nodes on the package and the four anchor nodes within the package; 2. the RSSI values were converted into distances using the log-distance path loss model; 3. the precise location of the package was determined by establishing a spatial triangle and solving the associated mathematical equations. This approach allows for the assessment of whether the radioactive cargo has been moved outside the compartment, indicating the occurrence of an unauthorized movement. It should be indicated that the presence of the multipath effect in wireless signal transmission introduces a notable challenge. As a result, the distances estimated from RSSI values are vulnerable to errors [22–24], which adversely affects the accuracy of determining the cargo location. Consequently, false and missed alarms may occur in identifying illegal movements of radioactive material packages. On the other

hand, due to the shielding effect of the metal carriage, wireless nodes installed outside the package may not receive signals from the anchor nodes within the cargo, let alone obtain RSSI values. Such instances cause the method not to function properly. Hence, the approach exhibits poor performance.

The conducted literature survey indicates that the existing detection methods deprive stability and accompany the failure risks of detection since the distance calculation based on RSSI generates errors that could lead to false and missed alarms. Consequently, it is of significant importance to develop a novel methodology to detect illegal movements of radioactive material packages steadily and dependably by succeeding with a high detection accuracy. A feasible solution to address the aforementioned challenges is to utilize the backpropagation (BP) neural network, which is a supervised learning algorithm that is commonly employed to solve various problems such as classification, regression, prediction, and pattern recognition problems [25]. In the field of nuclear energy, the BP neural network has been widely employed to monitor the operating state of nuclear systems, diagnose faults, identify nuclides, and optimize the design of reactors [26, 27]. Considering the superior characteristics of the BP neural network such as its proficiency in nonlinear fitting, adaptive learning, and handling multidimensional complex data, this scheme is adopted in the present study to detect unauthorized movements of radioactive material packages during transportation.

Similar to the study conducted by Zeng et al. [21], this article defines an unauthorized movement (or illegal movement) as any movement of radioactive cargo outside the truck's compartment during transportation. It is worth noting that although the standard BP neural network exhibits outstanding performance, it has some drawbacks such as slow converges and susceptibility to fall in local optimal solutions [28]. To resolve these problems, the Adam optimizer was employed in this article to optimize the standard model. As a result, a new Adam-optimized BP neural network model was developed to detect unauthorized movements of radioactive material packages. The main objective of the present study is to provide a reliable basis for alarm generation in the vehicle transportation security system. This article primarily focuses on the following aspects:

(1) Dataset Collection: several Wi-Fi modules were positioned on the inner wall of the cargo compartment and radioactive material transport packages. The RSSI sequence collected from the packages from the Wi-Fi modules inside the cargo compartment was measured after powering on all the modules. To establish a comprehensive dataset, the data collection procedure was repeatedly run at each time where the position of the packages is randomly adjusted, and then the corresponding RSSI values were recorded.

(2) Construction of the unauthorized movement detection model: several dynamic optimization algorithms were employed, and the results were compared. In this regard, the convergence speed and computational cost of the optimized BP neural network model were analyzed. Finally, an Adam-optimized BP neural network model was developed to detect unauthorized movements of radioactive materials.

(3) Experimental validation: experimental validation was carried out through the measured dataset, comparing and analyzing the changes of three indices, including the number of classification errors (NM), the accuracy rate (ACC), and the MacroF1 macro-mean of the unauthorized movement detection model before and after the optimization. The focus was on the accuracy of the model, as well as the false and missed alarm rate of the model.

3. Detection Model

3.1. BP Neural Network. The BP neural network is a multilayer feedforward neural network based on error backpropagation training. This model is one of the most widely used neural network models, which is commonly used in diverse applications [25]. The BP neural network primarily consists of three parts: the input layer, the hidden layer, and the output layer. Each layer contains several nodes, and the network weights reflect the connection status between layers. This model compares the actual output with the expected output in the output layer. If the results are inconsistent, the error is calculated and the error signal is propagated backward [29]. Then, the gradient descent algorithm continuously updates the network weights until the error meets the accuracy requirements.

Figure 1 shows the schematic structure of a typical three-layer BP neural network, in which $x_{1,\ldots,m,}$ and $\hat{y}_{1,\ldots,n}$ are input and output variables, respectively. Furthermore, v_{ij} and w_{ij} denote the weights between the nodes of the input and hidden layers and the hidden and output layers, respectively. The activation function of the hidden layer is ReLU with a bias term b_j, while that of the output layer is Softmax with a bias term θ_j. The forward propagation equation can be expressed as follows:

$$h_j = g\left(\sum_{i=0}^{m} v_{ij}x_i + b_j\right), \quad j = 1, 2, 3 \ldots m, \tag{1}$$

$$\hat{y}_j = f\left(\sum_{i=0}^{n} w_{ij}x_i + \theta_j\right), \quad j = 1, 2, 3, \ldots k. \tag{2}$$

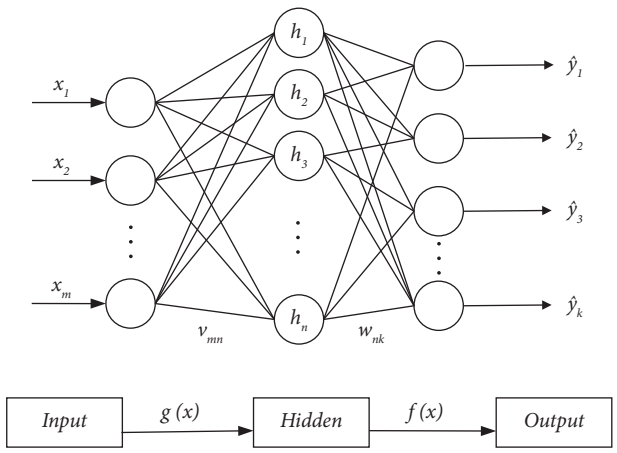

Figure 1: Schematic structure of the BP neural network ($g(x)$ and $f(x)$ are activation functions).

The BP neural network utilizes the gradient descent algorithm to optimize and update the network weights and bias terms. This algorithm is as follows:

$$v'_{ij} = v_{ij} - \alpha \frac{\partial J}{\partial v_{ij}}, \tag{3}$$

$$w'_{ij} = w_{ij} - \alpha \frac{\partial J}{\partial w_{ij}}, \tag{4}$$

$$b'_j = b_j - \alpha \frac{\partial J}{\partial b_j}, \tag{5}$$

$$\theta'_j = \theta_j - \alpha \frac{\partial J}{\partial \theta_j}, \tag{6}$$

where α represents the learning rate, with a default value of 0.01 [25]. This iterative process is repeated until the network converges to a satisfactory level of performance.

3.2. BP Neural Network Optimized by Adam Algorithm. The standard BP neural network algorithm is prone to oscillations during weight updates using the gradient descent algorithm, resulting in slower convergence rates and falling into local minima, thereby adversely affecting the model accuracy. To address these problems, the Adam optimization algorithm is adopted to optimize the standard BP neural network weight update algorithm [30]. This optimization algorithm dynamically adjusts the learning rate of each parameter by estimating the first-order and second-order moments of the gradients. It also incorporates momentum and adaptive learning rates to accelerate model training, improve network recognition accuracy, and reduce oscillations during convergence. For instance, the gradient descent algorithm updates $W^{[l]}$, which is the weight matrix between the hidden and output layers, through the following iterative calculations:

$$m_t = \eta_1 * m_{t-1} + (1 - \eta_1) * \mathrm{dW}^{[l]}_{t-1}, \tag{7}$$

$$n_t = \eta_2 * n_{t-1} + (1 - \eta_2) * \left(\mathrm{dW}^{[l]}_{t-1}\right)^2, \tag{8}$$

$$t = t + 1, \tag{9}$$

$$\widehat{m_t} = \frac{m_t}{1 - \eta_1^t}, \tag{10}$$

$$\widehat{n_t} = \frac{n_t}{1 - \eta_2^t}, \tag{11}$$

$$W^{[l]}_t = W^{[l]}_{t-1} - \alpha * \frac{\widehat{m_t}}{\sqrt{\widehat{n_t}} + \varepsilon}, \tag{12}$$

where m_t and n_t are first-order and second-order momentum terms, respectively, while $\widehat{m_t}$ and $\widehat{n_t}$ represent their bias-corrected estimates; $W^{[l]}_{t-1}$ denotes the value of the network weights of the t-1st iteration in the implicit and output layers; $\eta 1$ and $\eta 2$ are the default values of the hyperparameters; η_1^t and η_2^t represent the t-th power of η_1 and η_2, respectively.

Finally, the weights and biases are updated, and the weights $W^{[l]}_t$ for the t-th iteration are obtained as equation (12). Similarly the network weights $V^{[l]}_t$, biases $B^{[l]}_t$, and $\Theta^{[l]}_t$ between the input and hidden layers during the t-th iteration are updated as follows:

$$V^{[l]}_t = V^{[l]}_{t-1} - \alpha * \frac{\widehat{m_t}}{\sqrt{\widehat{n_t}} + \varepsilon}, \tag{13}$$

$$B^{[l]}_t = B^{[l]}_{t-1} - \alpha * \frac{\widehat{m_t}}{\sqrt{\widehat{n_t}} + \varepsilon}, \tag{14}$$

$$\Theta^{[l]}_t = \Theta^{[l]}_{t-1} - \alpha * \frac{\widehat{m_t}}{\sqrt{\widehat{n_t}} + \varepsilon}, \tag{15}$$

where $B^{[l]}_{t-1}$ and $\Theta^{[l]}_{t-1}$ denote the model bias at the t-1st iteration; $V^{[l]}_{t-1}$ is the network weight between the input and hidden layers at the t-1st iteration; α is the learning rate; ε is an infinitesimal real value.

3.3. Detection Model with an Adam-Optimized BP Neural Network

3.3.1. Model Feature Parameters and Label Definitions. Based on the analyses presented in the preceding sections, the fundamental concept of commonly used methods for identifying unauthorized relocation of radioactive material during transport revolves around continuous monitoring of its position within the cargo compartment. In this study, a Wi-Fi module was installed on the radioactive transportation parcel, while multiple Wi-Fi modules were deployed as access points (APs) within the transportation

compartment. Before the experiment, these Wi-Fi modules' operation mode and network parameters, including IP address and subnet mask, are required to be configured. Once powered on, the Wi-Fi module on the radioactive goods parcel receives the RSSI values from the multiple APs located within the compartment. These values can be organized into a sequence denoted as ($RSSI_1$, $RSSI_2$, ..., $RSSI_n$), where "n" represents the number of APs, which is 6 in the present study. Notably, distinct locations of the parcels yield different RSSI sequences. Therefore, these RSSI sequences can be used as the input feature parameters.

Given the concentration of security forces in the cab, diverting radioactive materials from the front of the truck would be unrealistic. Thus, RSSI data collection from this specific orientation was omitted. During the experiment, with the truck in the center, the area is divided into four distinct regions with unique labels: the interior, the left side, the right side, and the rear area. The neural network's output value corresponds to the region code, wherein a unique code is allocated to each label. Table 1 provides a mapping between the labels and respective regions.

3.4. Model Architecture Design. The proposed model utilizes a 3-layer Adam-optimized BP neural network. In this model, the hidden layer consists of 32 neurons, while the input layer comprises 6 neurons corresponding to the RSSI values received from 6 APs within the compartment. The output layer consists of 4 neurons and employs Softmax activation to classify the region into four distinct regions. The hidden and output layers employ ReLU and Softmax activation functions, respectively. Figure 2 illustrates the structure of the Adam-optimized BP neural network model for unauthorized movement detection of radioactive material packages.

The training dataset encompasses 70% of the collected dataset, while the remaining 30% is allocated as the test data. Once the model is trained, inputting the RSSI values gathered from the six access points received from the radioactive transportation package empowers the model to generate the corresponding region code for the parcel. Consequently, the specific location of the radioactive parcel can be determined accordingly. If the radioactive parcel is detected outside the truck's compartment, it indicates an illegal movement has occurred.

4. Experiment

4.1. Hardware Components. The RSSI dataset was collected using seven 51 mm ∗ 28 mm Wi-Fi modules, as shown in Figure 3(a). Each module featured an onboard 2.4 GHz Wi-Fi chip antenna and was equipped with a 32-bit low-power dual-core ESP32-WROOM-32 as the core processor. The Wi-Fi modules were powered by a 3.7 V lithium-ion battery. These modules are small, cost-effective, and efficient Wi-Fi modules that offer exceptional performance.

Table 1: Regional label classifications.

Regions	Labels
The interior of the truck	1
The left side of the truck	2
The rear of the truck	3
The right side of the truck	4

4.2. Experimental Environment. The experimental truck's compartment is 3.00 m long, 1.60 m wide, and 1.55 m high. The compartment's roof is situated at a height of 2.3 m above the ground. The experiment was conducted in three steps: firstly, six anchor nodes were arranged inside the compartments affixed directly with transparent adhesive paste. These anchor nodes were set to operate in the AP mode that broadcast wireless signals for other terminals to scan and obtain signal strength. Figure 4 illustrates the installation positions of the anchor nodes. Secondly, one additional Wi-Fi module was designated as the mobile node, simulating a node mounted on the radioactive material transporting container. The mobile node was operated in the STA (station) + AP mode. Once the node was powered on, it automatically scanned and obtained the RSSI values from the six anchor nodes and transmitted the collected data to a PC via the TCP protocol. Finally, the received RSSI data was read and stored on the PC using NetAssist V5.0.2 software.

Based on the measurement results, the mobile node established communication with the anchor node located in the rear area of the truck at a maximum distance of 8 m. However, when the mobile node was positioned on the left or right side of the truck, the connection to the anchor node was lost at a distance of approximately 5 m from the compartment. Notably, the mobile node hardly detected signals from the anchor node inside the compartment when positioned on the front side. Accordingly, the experimental area was divided into four sections: the interior of the truck's compartment, the area within 5 m to the left and right of the truck, and the region within 8 m from the rear of the truck. During the experiment, the mobile node was randomly moved within these four regions, collecting RSSI values from the six anchor nodes within the compartment at each point. Additionally, the height of the mobile node at the same measurement point was measured to simulate scenarios where packages of different volumes of radioactive materials were illegally moved outside the truck, thereby enriching the dataset. In total, 10113 data points were collected during the experiment. Figure 5 shows photographs of the experimental site.

4.3. Data Preprocessing. RSSI values are affected by a variety of interfering factors such as multipath, scattering, obstacles, and metal shielding that are typically present in the environment. To reduce the measurement error caused by the interference, multiple measurements are conducted at the same location when collecting data. During the experiment,

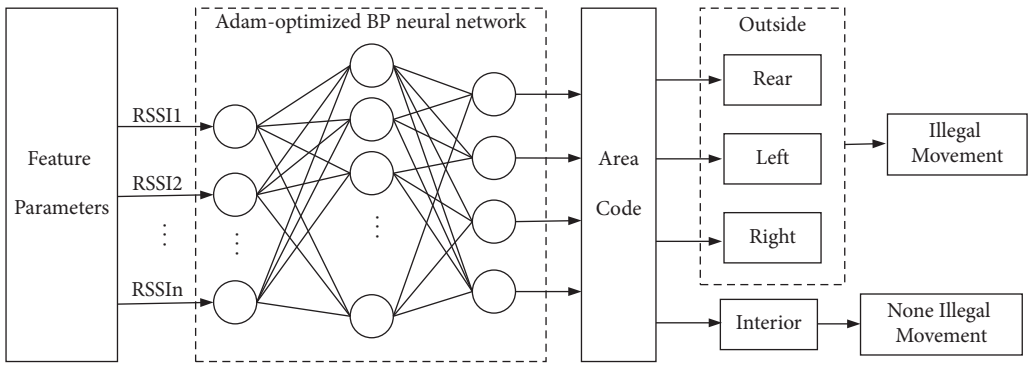

Figure 2: Structure of the Adam-optimized BP neural network model for unauthorized movement detection of radioactive material packages.

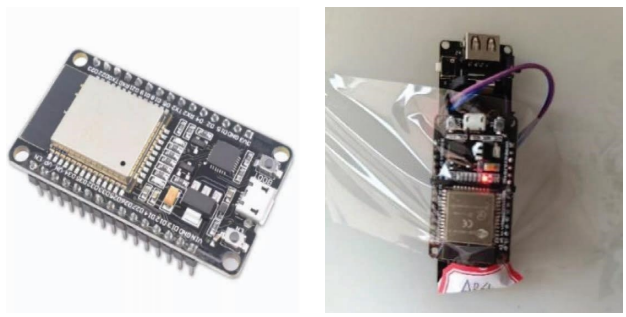

(a) (b)

Figure 3: Wi-Fi module: (a) the front view of the module and (b) Wi-Fi module attached to the inner wall of the truck's compartment.

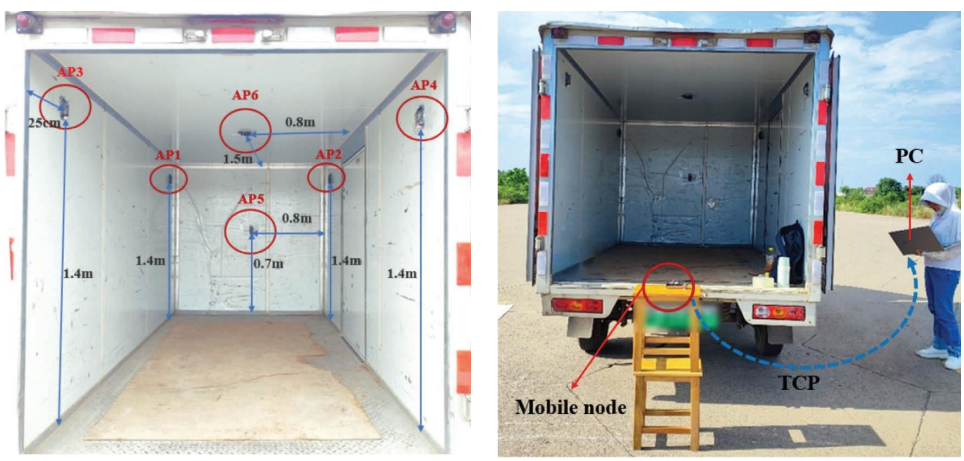

(a) (b)

Figure 4: Experimental site: (a) anchor node installation diagram in the compartment and (b) mobile node communication schematic diagram.

the mobile node reads 20 consecutive RSSI values from each AP at each measurement point, creating a set of RSSI values. On the PC side, a Gaussian filter is applied to the collected RSSI data from the same AP to obtain the final RSSI value. This value is then stored in the sample dataset for subsequent training and testing of the neural network model.

The main concept of applying Gaussian filtering is to select the RSSI value of the high probability region as the effective value and then calculate its geometric mean. This method effectively reduces the errors caused by small probability events and improves the accuracy of the measured data. Based on empirical observations, RSSI values

(a) (b) (c) (d)

Figure 5: Experimental site in four sections of the truck: (a) left side, (b) rear side, (c) interior area, and (d) right side.

follow a Gaussian distribution [31], with the probability density function in the form as follows:

$$f(x) = \frac{1}{\sigma\sqrt{2\pi}}[ee]\frac{(x-\mu)^2}{2\sigma^2}, \tag{16}$$

where the mean μ and variance σ^2 are expressed as

$$\mu = \frac{1}{m}\sum_{i=1}^{m}\mathrm{RSSI}_i, \tag{17}$$

$$\sigma^2 = \frac{1}{m-1}\sum_{i=1}^{m}\left(\mathrm{RSSI}_i - \mu\right)^2. \tag{18}$$

Therefore, μ and σ^2 can be calculated by introducing the measured RSSI values into equations (17) and (18). To compute the Gaussian distribution corresponding to each set of RSSI, the obtained μ and σ^2 are applied to the density function of the Gaussian distribution, as defined in equation (16). The RSSI values were selected according to the sigma principle of the Gaussian distribution, and then the average was taken over k RSSI values. Finally, the desired RSSI value can be obtained from the following expression:

$$\mathrm{RSSI} = \frac{1}{k}\sum_{i=1}^{k}\mathrm{RSSI}_i. \tag{19}$$

After applying Gaussian filtering, the final RSSI dataset can be obtained. This dataset contained 10113 samples collected from random locations within four regions. Table 2 provides details of the data distribution. Due to shielding and obstruction caused by the compartment, the mobile node was unable to scan signals from certain APs in specific areas on the left and right sides near the front of the truck. As stated previously, the method outlined in [13] fails to provide a reliable means of detecting unauthorized movements of the radioactive material packages under these circumstances. In our study, these RSSI values were adjusted to a minimal value of −200 dBm in the dataset during the data preprocessing stage and served as a vital component in the training and testing sets of the detection model. Moreover, even if the packages were in areas where certain APs' signals were blocked, the proposed detection model could remain capable of effectively detecting the unauthorized movements of packages.

5. Results and Discussion

5.1. Comparison of Multiple Optimization Algorithms. After establishing the dataset, the model was trained to detect unauthorized movements of radioactive material packages. Data processing, as well as model construction, was performed on the PyTorch framework within the PyCharm integrated development environment.

To validate the superiority of the Adam-optimized BP neural network algorithm, it was compared with the standard BP neural network and BP neural networks optimized by other algorithms such as RMSProp, AdaGrade, and AdaDelta that exhibit adaptive learning capabilities. The results illustrated in Figure 6 show that the Adam and RMSProp optimization algorithms outperform the other algorithms in terms of cost and convergence rate. Furthermore, it is found that the Adam optimization algorithm exhibits a clear advantage over the RMSProp optimization algorithm regarding computational costs. Therefore, it is concluded that the utilization of the Adam algorithm for optimizing the BP neural network confers significant advantages.

5.2. Analysis of Experimental Results. The classification prediction was performed using an Adam-optimized BP neural network model with a learning rate of 0.01. The dataset contained 10113 pieces of data, 70% of which is allocated to a training set and 30% to a testing set for experimental validation. The output results were classified into four categories: the interior, the left side, the right side, and the rear of the truck. The evaluation metrics were the number of misclassifications (NM), accuracy (ACC), and the macro-average of F1 scores (MarcoF1). ACC is defined as the ratio of correctly classified instances to the total number of instances and can be mathematically expressed as follows:

$$\mathrm{ACC} = \frac{P_{\mathrm{test}}}{S_{\mathrm{test}}} * 100\%, \tag{20}$$

Table 2: Data distribution.

Regions	Number of samples	Percentage (%)
The interior of the truck	2412	23.9
The left side of the truck	2507	24.7
The rear of the truck	2928	29.0
The right side of the truck	2266	22.4

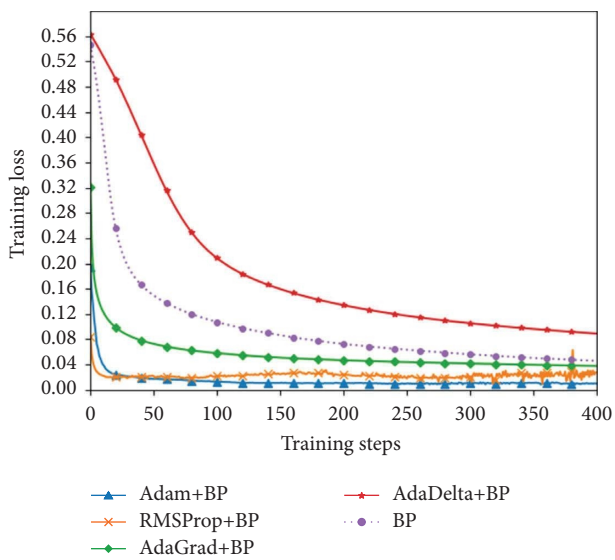

Figure 6: Performance of various optimization algorithms.

where P_{test} is the number of correctly classified instances and S_{test} is the total number of test instances.

The MarcoF1 macro-average is an index, which is widely used to measure the accuracy and stability of multi-classification models while considering both precision rate and recall rate. In this paper, the output results form a four-classification problem. To calculate the MarcoF1 macro-average, it is necessary to decompose it into four binary classifications. The F1 score is computed for each binary classification, and then the average of the four F1 scores is calculated to obtain the MarcoF1 macro-average. This approach ensures the comprehensive evaluation of the model's performance across all classes. The MarcoF1 index can be obtained from the following expression:

$$\text{F1}^{(i)} = \frac{2 * P^{(i)} * R^{(i)}}{P^{(i)} + R^{(i)}}, \tag{21}$$

$$\text{MacroF1} = \frac{1}{4} \sum_{i=1}^{4} 2 * \frac{P^{(i)} * R^{(i)}}{P^{(i)} + R^{(i)}}, \tag{22}$$

where $P^{(i)}$ and $R^{(i)}$ are the precision and recall of class i, respectively.

The experiment compared the number of NM, ACC, and MarcoF1 macro-average values between the BP neural network and the Adam-optimized BP neural network models. As shown in Table 3, the results reveal that as the number of training epochs increases, the classification accuracy of both models on the test data improves. For the same number of training epochs, the Adam-optimized BP neural network demonstrates higher accuracy and MarcoF1 macro-average values compared with the BP neural network. Additionally, the Adam-optimized model has substantially fewer misclassifications. Specifically, when the number of epochs was set to 200, the Adam-optimized BP neural network displayed a 28.6% reduction in the number of misclassifications compared to the standard BP neural network. The gap between the NM, ACC, and MarcoF1 macro-average of the Adam-optimized BP neural network and the BP neural network models gradually exhibits a negative correlation with the number of epochs. However, the Adam-optimized BP neural network model consistently outperforms the BP neural network model across these evaluation metrics.

The classification results were converted into two categories: "inside the truck's compartment" and "outside the truck's compartment" by merging the classifications for the left side, right side, and rear of the truck. The classification "outside the truck's compartment" signifies that an unauthorized movement has occurred, which is also referred to as an abnormal event. On the other hand, the classification "inside the truck's compartment" indicates that there was no unauthorized movement, so it is also called a normal event. The output results are crucial evidence for alarming the onboard transportation security system. In cases where radioactive materials are moved outside but the model incorrectly classifies them as "inside the truck's compartment," the system fails to generate an alarm. This case is known as a missed alarm. Conversely, if the radioactive materials are inside the compartment, but the model predicts it as "outside the truck compartment," and a false alarm is triggered. The missed alarm rate and false alarm rate are defined as follows:

$$\text{False alarm rate} = \frac{N_{IO}}{N_I} * 100\%, \tag{23}$$

$$\text{Missed alarm rate} = \frac{N_{OI}}{N_O} * 100\%, \tag{24}$$

where N_{IO} is the number of samples inside the truck misclassified as outside the truck or the number of normal events misclassified as abnormal events; N_I is the actual total number of samples inside the truck or the actual total number of the normal event; N_{OI} is the number of samples outside the truck misclassified as inside the truck or the number of abnormal events misclassified as normal events; N_O is the actual total number of samples outside the truck, or the actual total number of the abnormal event.

The models were trained for 300 epochs with a learning rate of 0.01. The confusion matrices of the standard BP neural network model and the Adam-optimized BP neural network model are shown in Figure 7. It is observed that in the classification obtained from the standard BP neural network, 8 of the 727 test points inside the truck compartments were misclassified, and 24 of the 2307 test points outside the truck's compartment were mispredicted. Accordingly, the overall classification accuracy was 98.95%. Meanwhile, the rates of missed and false alarms were 0.79% and 0.26%, respectively. Figure 7(b) shows that when using

Table 3: Experimental results obtained from BP and Adam-optimized BP algorithms.

Epochs	BP			Adam-optimized BP		
	NM	ACC (%)	MacroF1 (%)	NM	ACC (%)	MacroF1 (%)
50	93	96.93	97.07	72	97.63	97.69
100	91	97.03	97.16	69	97.73	97.79
200	77	97.46	97.54	65	97.89	97.95
400	75	97.53	97.60	64	97.96	98.01

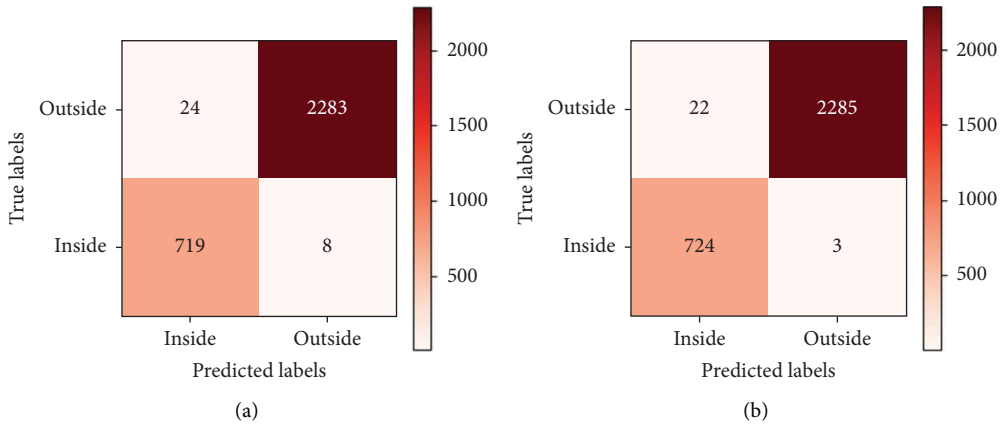

Figure 7: Binary confusion matrix of the model before and after optimization: (a) standard BP neural network model and (b) Adam-optimized BP neural network model.

the Adam-optimized BP neural network model for detection, only 3 of the 727 test points inside the truck compartment were correctly classified, resulting in a false alarm rate of 0.1%. However, 22 of the 2307 test points outside the truck compartment were wrongly classified as the interior, resulting in a missed alarm rate of 0.72%. Accordingly, the overall classification accuracy of the model was 99.17% indicating that the modified model outperforms the standard model.

6. Conclusions

To reduce the rates of false and missed alarms in detecting unauthorized movements of radioactive material shipments, an Adam-optimized BP neural network model was proposed in the present study. The developed model was applied to detect unauthorized movements of radioactive material packages. It was found that the Adam-optimized BP neural network model improves classification accuracy and macro-average values compared with the standard BP neural network algorithm. When the output results were categorized into 4 classes: they are the interior, left and right sides, and the rear sections of a truck. The results revealed that the maximum reduction in classification errors is 28.6%. Experimental results indicate that when classifying the output data as whether inside or outside of the truck compartment, the proposed model achieves an accuracy rate of 99.17%, a missed alarm rate of 0.72%, and a false alarm rate of 0.1% in detecting unauthorized movement of radioactive materials.

This article demonstrates that the developed method exhibits high accuracy and stability in detecting unauthorized movements, effectively avoids false alarms and achieves a very low missed alarm rate. This method holds significant potential for enhancing the security of transporting radioactive materials. The developed method addresses various concerns such as losses, theft, and malicious incidents. This approach contributes to enhancing overall transportation security levels.

Data Availability

The data used to support the findings of this study are available from the corresponding author on request.

Conflicts of Interest

The authors declare that there are no conflicts of interest regarding this publication.

Acknowledgments

This study was funded by China's 13th Five-Year Nuclear Energy Development Project, "Individual Self-Security Intelligence of Radioactive Material."

References

[1] IAEA, "Transport security," 2013, https://www.iaea.org/topics/transport-security.

[2] IAEA, "IAEA incident and trafficking Database (ITDB)," 2023, https://www.iaea.org/sites/default/files/22/01/itdb-factsheet.pdf.

[3] Nrc Library, "Reports associated with events," 2020, https://www.nrc.gov/reading-rm/doc-collections/event-status/event/2020/20200217en.html.

[4] Nrc Library, "Reports associated with events," 2019, https://www.nrc.gov/reading-rm/doc-collections/event-status/event/2019/20190809en.html.

[5] M. Goetstouwers and T. Sauer, "The security of transport of radioactive and nuclear material in Belgium," *Journal of Risk Research*, vol. 25, no. 4, pp. 439–452, 2022.

[6] K. Vetter, "Initiative to enhance radiological resilience," in *Nuclear Terrorism and National Preparedness*, pp. 189–200, Springer Netherlands, Dordrecht, Netherlands, 2015.

[7] Iaea, *Security of Radioactive Material in Transport: Implementing Guide*, International Atomic Energy Agency, Vienna, Austria, 2020.

[8] A. J. Gilbert, B. S. McDonald, S. M. Robinson, K. D. Jarman, T. A. White, and M. R. Deinert, "Non-invasive material discrimination using spectral x-ray radiography," *Journal of Applied Physics*, vol. 115, no. 15, 2014.

[9] H. C. Tsai, K. Chen, Y. Y. Liu, and J. M. Shuler, "Demonstration (DEMO) of radiofrequency identification (RFID) system for tracking and monitoring of nuclear materials," *Packaging, Transport, Storage and Security of Radioactive Material*, vol. 21, no. 2, pp. 91–102, 2010.

[10] J. Anderson, H. Lee, P. De Lurgio et al., "Tracking and monitoring with dosimeter-enabled ARG-US RFID system," in *Proceedings of the Waste Management Symposia*, pp. 1–9, Phoenix, AZ, USA, February, 2012.

[11] Y. Y. Liu, B. Craig, H. Mehta, K. Byrne, Z. Han, and J. M. Shuler, "ARG-US traveler for tracking and monitoring conveyances," in *Proceedings of the INMM 59th Annual Meeting*, pp. 22–26, Washington, DC, USA, July, 2018.

[12] Y. Y. Liu, B. Craig, and J. Shuler, "ARG-US remote monitoring systems for enhancing security of radioactive material," in *Proceedings of the IAEA International Conference on the Security of Radioactive Material: The Way Forward for Prevention and Detection*, Vienna, Austria, December, 2018.

[13] L. Vander Wal, B. Craig, K. Byrne, Y. Y. Liu, and J. M. Shuler, "Geofence for ARG-US TRAVELER during RAM shipment," in *Proceedings of the 19th International Symposium on the Packaging and Transportation of Radioactive Materials (PATRAM 2019)*, New Orleans, LA, USA, August, 2019.

[14] B. Deb, "Iterative estimation of location and trajectory of radioactive sources with a networked system of detectors," *IEEE Transactions on Nuclear Science*, vol. 60, no. 2, pp. 1315–1326, 2013.

[15] S. Bauk, "Modelling radioactive materials tracking in sea transportation by RFID technology," *TransNav, the International Journal on Marine Navigation and Safety of Sea Transportation*, vol. 14, no. 4, pp. 1009–1014, 2020.

[16] Z. Liu and C. J. Sullivan, "Urban source detection with mobile sensor networks enhanced with machine learning algorithms," in *Proceedings of the 2016 IEEE Nuclear Science Symposium, Medical Imaging Conference and Room-Temperature Semiconductor Detector Workshop (NSS/MIC/RTSD)*, pp. 1-2, IEEE, Strasbourg, France, October, 2016.

[17] M. S. Bandstra, T. J. Aucott, E. Brubaker et al., "RadMAP: the radiological multi-sensor analysis platform," *Nuclear Instruments and Methods in Physics Research Section A: Accelerators, Spectrometers, Detectors and Associated Equipment*, vol. 840, pp. 59–68, 2016.

[18] R. R. Flanagan, L. J. Brandt, A. G. Osborne, and M. R. Deinert, "Detecting nuclear materials in urban environments using mobile sensor networks," *Sensors*, vol. 21, no. 6, p. 2196, 2021.

[19] R. R. Flanagan, A. G. Osborne, and M. R. Deinert, "Data synthesis improves detection of radiation sources in urban environments," *Nuclear Instruments and Methods in Physics Research Section A: Accelerators, Spectrometers, Detectors and Associated Equipment*, vol. 1058, Article ID 168821, 2024.

[20] T. Zeng, X. Yang, Y. Wan, Z. Liu, and P. Jiang, "Single-vehicle transportation security system of radioactive materials based on group relationship to prevent loss and theft," *Science and Technology of Nuclear Installations*, vol. 2021, Article ID 6649649, 9 pages, 2021.

[21] T. Zeng, X. Yang, Y. Wan, P. Jiang, and L. Zhenghai, "Detection of illegal movement in radioactive material transportation security systems," *Science and Technology of Nuclear Installations*, vol. 2021, Article ID 6670114, 9 pages, 2021.

[22] G. Zanca, F. Zorzi, A. Zanella, and M. Zorzi, "Experimental comparison of RSSI-based localization algorithms for indoor wireless sensor networks," in *Proceedings of the workshop on Real-world wireless sensor networks*, pp. 1–5, Padova, Italy, April, 2008.

[23] S. Sadowski and P. Spachos, "Rssi-based indoor localization with the internet of things," *IEEE Access*, vol. 6, pp. 30149–30161, 2018.

[24] H. Liu, H. Darabi, P. Banerjee, and J. Liu, "Survey of wireless indoor positioning techniques and systems," *IEEE Transactions on Systems, Man, and Cybernetics, Part C (Applications and Reviews)*, vol. 37, no. 6, pp. 1067–1080, 2007.

[25] J. T. Lalis, B. D. Gerardo, and Y. Byun, "An adaptive stopping criterion for backpropagation learning in feedforward neural network," *International Journal of Multimedia and Ubiquitous Engineering*, vol. 9, no. 8, pp. 149–156, 2014.

[26] H. Yang, D. Wang, and D. Wang, "An overview of the application of neural network algorithm in the nuclear field of China," *Nuclear Science Technology*, vol. 08, no. 01, pp. 19–34, 2020.

[27] J. He, X. Tang, P. Gong et al., "Rapid radionuclide identification algorithm based on the discrete cosine transform and BP neural network," *Annals of Nuclear Energy*, vol. 112, pp. 1–8, 2018.

[28] Z. Dong, J. Jiang, and X. Zhao, "Detection of subway air conditioning environment modes using BP neural network optimized by Adam," *Electronic Measurement Technology*, vol. 24, pp. 111–117, 2022.

[29] A. Yang, Y. Zhuansun, C. Liu, J. Li, and C. Zhang, "Design of intrusion detection system for internet of things based on improved BP neural network," *IEEE Access*, vol. 7, pp. 106043–106052, 2019.

[30] D. P. Kingma and J. Ba, "Adam: a method for stochastic optimization," 2014, https://arxiv.org/abs/1412.6980.

[31] K. Elgui, P. Bianchi, F. Portier, and O. Isson, "Learning methods for RSSI-based geolocation: a comparative study," *Pervasive and Mobile Computing*, vol. 67, Article ID 101199, 2020.